Article ID: 1000-7032(2024)01-0001-10

Patterned Vapor Deposited Perovskite Light Emitting Diodes *via* Phosphine Oxide Passivation

LIU Nian[1], LUO Jiajun[1*], DU Peipei[2],
LIU Zhengzheng[3,4], DU Juan[3,4], TANG Jiang[1*]

(1. *Wuhan National Laboratory for Optoelectronics (WNLO), Huazhong University of Science and Technology (HUST), Wuhan* 430074, *China*;
2. *School of Integrated Circuits, Huazhong University of Science and Technology (HUST), Wuhan* 430074, *China*;
3. *School of Physics and Optoelectronic Engineering, Hangzhou Institute for Advanced Study, UCAS, Hangzhou* 310024, *China*;
4. *State Key Laboratory of High Field Laser Physics and CAS Center for Excellence in Ultra-Intense Laser Science, Shanghai Institute of Optics and Fine Mechanics, Chinese Academy of Sciences, Shanghai* 201800, *China*)

* *Corresponding Authors, E-mail: luojiajun@hust. edu. cn; jtang@hust. edu. cn*

Abstract: Thermal evaporation is promising for bringing perovskite light-emitting diodes (PeLEDs) towards commercial display applications. However, vapor-deposited perovskites exhibit low photoluminescence quantum yield (PLQY) due to unpassivated defect states. Here, we report a method of introducing passivating ligands into perovskites through an *in-situ* co-evaporation technique. The phosphonate groups coordinated with unsaturated sites, passivating the grain boundary defects in perovskite and suppressing trap states. LED devices based on perovskite films prepared with the optimal ratio exhibited a maximum EQE of 6. 3% and a maximum brightness of 35 642 cd/m^2. Furthermore, by employing a fully vacuum-based device fabrication process, high-resolution PeLEDs with a maximum EQE of 5. 0% at 312 pixels per inch (ppi) were achieved. In conclusion, this study provides useful guidance for defect passivation in thermal-evaporated PeLEDs, demonstrating the great potential and commercial prospects of thermal-evaporation PeLEDs in efficiency and brightness enhancement.

Key words: perovskite light-emitting diodes; thermal evaporation; defect passivation; patterning
CLC number: TN312. 8 **Document code**: A **DOI**: 10. 37188/CJL. 20230231

基于膦氧化物钝化的热蒸发像素化钙钛矿发光二极管

刘 念[1], 罗家俊[1*], 杜培培[2], 刘征征[3,4], 杜 鹃[3,4], 唐 江[1*]

(1. 华中科技大学 武汉光电国家研究中心, 湖北 武汉 430074; 2. 华中科技大学 集成电路学院, 湖北 武汉 430074;
3. 国科大杭州高等研究院 物理与光电工程学院, 浙江 杭州 310024;
4. 中国科学院 上海光学精密机械研究所, 强场激光物理国家重点实验室, 上海 201800)

摘要: 热蒸发法是实现钙钛矿发光二极管商业化显示应用的可靠技术。然而,热蒸发沉积的钙钛矿薄膜的PLQY经常较低,并且钝化手段不如溶液法丰富。本文报道了一种通过原位共蒸技术将钝化剂引入钙钛矿层的方法,这种方法能够钝化真空沉积钙钛矿中的缺陷,增强辐射复合,并提高钙钛矿的PLQY。氧膦基团与不饱和位点形成配位络合,钝化了钙钛矿的晶界缺陷,并抑制了带尾态缺陷。基于最佳比例的钙钛矿薄膜所制

收稿日期: 2023-10-08; **修订日期**: 2023-10-23
基金项目: 国家自然科学基金(61725401,62104077,61875211,62050039,62004075,62005089); 湖北省自然科学研究基金创新研究组(2020CFA034); 博士后创新人才研究计划(BX20220119)
Supported by National Natural Science Foundation of China(61725401,62104077,61875211,62050039,62004075,62005089); Fund for Innovative Research Groups of the Natural Science Foundation of Hubei Province(2020CFA034); Post-doctoral Innovative Talent Support Program(BX20220119)

备的LED器件表现出最大6.3%的EQE,最大亮度为35 642 cd/m^2。更进一步地,基于全真空的器件制备工艺,获得了最大EQE为5.0%的312 ppi高分辨率PeLEDs。总之,本文为热蒸发PeLEDs的缺陷钝化提供了有用的指导,证明热蒸发PeLEDs在效率和亮度提升方面具有巨大潜力,并具备商业化前景。

关 键 词:钙钛矿发光二极管;热蒸发;缺陷钝化;像素化

1 Introduction

Metal halide perovskites have attracted significant interest due to their excellent color purity, tunable emission wavelength covering the visible range, and low material cost[1-6]. In recent years, there have been remarkable advancements in the device performance and operational stability of perovskite light-emitting diodes (PeLEDs), driven by continuous innovation and breakthroughs in material properties and device structures[7-15]. However, the widely used solution spin-coating method in laboratories for perovskite deposition has limitations in terms of fabrication area and process repeatability[16-20]. Vacuum thermal evaporation, a technology extensively employed in OLED panel production lines, offers a promising solution for large-scale commercial production of PeLEDs, as it enables scale-up deposition, high repeatability, and precise deposition[17,21-24].

The research on vapor-deposited PeLEDs started relatively late, focusing mainly on efficiency enhancement strategies such as optimizing material composition, and process parameters, and introducing interfacial layers[23, 25-30]. These strategies aimed to improve the photoluminescence quantum yield (PLQY) of the perovskite film and enhance the electron-hole injection balance in the LED. In the optimization of vapor-deposited perovskite layers, commonly used techniques include introducing quasi-2D structures and encapsulating with Cs_4PbBr_6 to create dielectric confinement. While these methods increased the exciton binding energy and PLQY by enhancing carrier recombination probability, the improvement is limited and may affect the carrier transport within the perovskite layer. Compared to enhancing radiative recombination in the perovskite, suppressing defect-assisted non-radiative recombination in the perovskite can better improve the PLQY while maintaining efficient carrier transport[31-32]. The published studies have shown the presence of halide vacancies in the lattice and surface defects in pristine perovskite films[5-6,33]. In solution-based methods, extensive research has been conducted to passivate these defects using Lewis-base additive molecules, such as organic ligands and conductive polymers, to interact with under-coordinated Pb^{2+} ions[7,34-37].

In this study, bis(p-chlorophenyl) phenylphosphine oxide (Cl-TPPO) was first introduced *in situ* during the thermal evaporation deposition process of perovskite to achieve defect passivation and enhanced radiative recombination. The phosphine oxide with phosphine oxide group effectively complexes with undercoordinated Pb^{2+}, suppressing defect-assisted non-radiative recombination and controlling the high-energy and disordered crystallization process during thermal evaporation. By optimizing the ratio of raw materials during the evaporation process, the growth kinetics of the perovskite film were also optimized, leading to an improvement in radiative recombination efficiency. Based on the emission-enhanced perovskite layer, the LED device structure was carefully selected and optimized, resulting in thermal-evaporated green PeLEDs with a maximum EQE of 6.3% and 312 pixels per inch (ppi) high-resolution perovskite LEDs with an EQE of 5.0%.

2 Experiment

2.1 Materials

Indium tin oxide (ITO) glasses were purchased from Liaoning Youxuan New Energy Technology Co., Ltd. Cesium bromide (CsBr, 99.99%) and lead bromide (PbB_2, 99.99%) were purchased from Aladdin Reagent Ltd. Bis(p-chlorophenyl) phenylphosphine oxide (Cl-TPPO, 96%) was purchased from Alfa chemistry. 4,4′-Bis[N-(1-naphthyl)-N-phenylamino]biphenyl (NPB, >99.5%) and 1,3,5-tris

(1-phenyl-1H-benzimidazol-2-yl)benzene (TPBi, >99.5%) were purchased from Taiwan Luminescence Technology Co., Ltd. Molybdenum trioxide (MoO_3, >99.9%) and lithium fluoride (LiF, >99.99%) were purchased from Sigma-Aldrich(Shanghai) Trading Co., Ltd. Aluminum pellets (Al, 99.999%) were purchased from Zhongnuo Advanced Material (Beijing) Technology Co., Ltd.

2.2 Deposition of Perovskite Film

The deposition of perovskite was carried out by simultaneously evaporating multiple sources. The evaporation rates of the sources were monitored by quartz microbalance and calibrated with a stylus profiler. After optimization, the deposition ratios and rates of CsBr, $PbBr_2$, and Cl-TPPO were determined to be 0.01, 0.01, 0.006 nm/s, respectively. During the deposition process of perovskite, the substrate rotated at a rate of 8 r/min to ensure the uniformity of the perovskite film. The vacuum chamber maintained a vacuum degree below 10^{-4} Pa to ensure the reproducibility of the deposition process.

2.3 Device Fabrication

The etched ITO glasses were subjected to sequential immersion and ultrasonic cleaning with surfactant, acetone, isopropanol, and ethanol, they were dried by N_2 blowing and transferred to thermal evaporation equipment for the deposition of functional layers. The functional layers NPB and MoO_3 were deposited at evaporation rates of 0.2 nm/s and 0.04 nm/s, followed by the deposition of the perovskite layer, as mentioned above. TPBi, LiF, and Al were deposited at evaporation rates of 0.1 nm/s, 0.02 nm/s, and 0.3 nm/s, respectively, onto the rotating substrate to achieve the desired thickness.

2.4 Characterizations

The Shimadzu Solidspec-3700 spectrophotometer was used to measure the absorption spectra, while the Hitachi F-7000 fluorescence spectrometer was utilized for recording the PL spectra. The Zolix OmniFluo spectrofluorometer with a calibrated integrating sphere from Labsphere was employed to determine the absolute PLQY. The PL lifetime was measured using an Edinburgh Instruments Ltd EPL-370. X-ray photoelectron spectroscopy (XPS) was conducted using a Shimadzu-Kratos AXIS-ULTRA DLD-600W photoelectron spectrometer from Japan. Transient absorption(TA) spectroscopy experiments were performed using a commercial Helios-EOS Ultrafast system. The tests of PL, PLQY, TRPL, and TA were all performed under excitation light at 365 nm. The characterization of the PeLEDs was carried out in a N_2 glove box. A commercial measurement system (XPQY-EQE, Guangzhou Xi Pu Optoelectronics Technology) equipped with an integrating sphere was used to simultaneously record the current density *versus* voltage, luminance *versus* voltage, and EQE *versus* current density curves. This measurement system was calibrated by the National Institute of Standards and Technology(NIST) using halogen lamps.

3 Results and Discussion

The optical properties of the perovskite films before and after the addition of Cl-TPPO are compared and shown in Fig. 1. The test results indicate that the addition of Cl-TPPO does not affect the absorption edge of the perovskite, and the composition of perovskite remained unchanged. The photofluo-

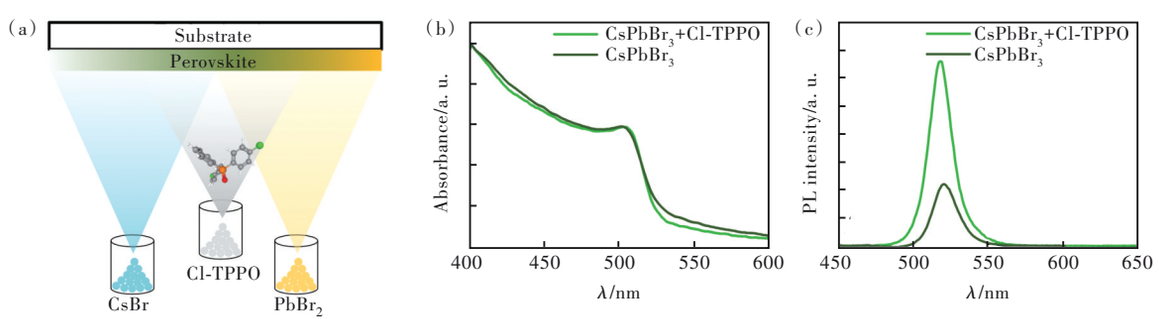

Fig. 1 (a) Schematic diagram of co-evaporation deposition. (b) UV-Vis absorption spectra. (c) PL spectra of $CsPbBr_3$ films without and with Cl-TPPO

rescence (PL) intensity of the films is significantly enhanced, with the emission peak shifting from 520.7 nm to 518.2 nm, and the full width at half maximum (FWHM) decreasing from 20 nm to 18 nm. Overall, the optical properties of the perovskite thin film have been improved.

The time-resolved PL (TRPL) and PLQY tests performed on perovskite films before and after Cl-TPPO addition are shown in Fig. 2. The addition of Cl-TPPO would increase the PLQY of perovskite films from 21% to 57%, and the improved PLQY would contribute to the EQE improvement of PeLEDs devices. In the transient PL spectroscopy test, the film of $CsPbBr_3$+Cl-TPPO showed a longer PL lifetime, and the PL lifetime was calculated by double exponential fitting and average lifetime according to the following formula[31]:

$$y(t) = \sum_i A_i \exp(-t/\tau_i), \tag{1}$$

$$\tau_{avg} = \frac{A_1 \times \tau_1^2 + A_2 \times \tau_2^2}{A_1 \times \tau_1 + A_2 \times \tau_2}, \tag{2}$$

the life-fitting results are shown in Tab. 1. The addition of Cl-TPPO increased the average lifetime of perovskite films from 6.39 ns to 7.79 ns.

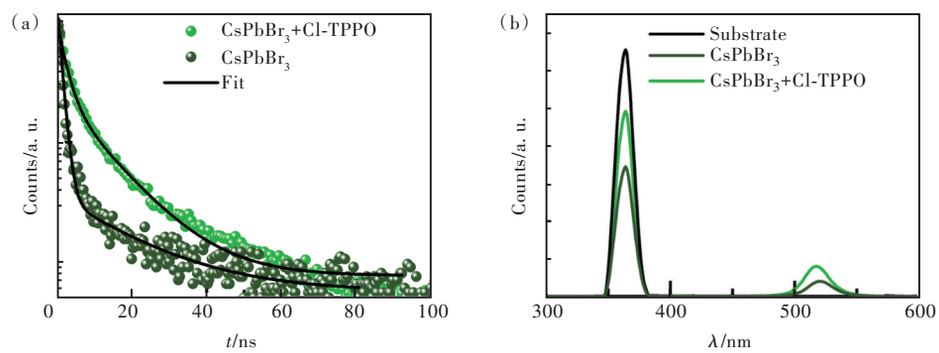

Fig.2 TRPL(a) and PLQY(b) test results of perovskite films before and after Cl-TPPO addition

Tab. 1 Double exponential fitting results of PL attenuation curves of perovskite film without and with Cl-TPPO addition

	A_1	τ_1/ns	A_2	τ_2/ns	τ_{avg}/ns
$CsPbBr_3$	1.26	1.11	0.03	19.12	6.39
$CsPbBr_3$+Cl-TPPO	0.86	2.14	0.25	11.43	7.79

By substituting the average lifetime and PLQY (η_{PLQY}) into the equations below, the proportion and rate of radiation and non-radiation recombination in perovskite films can be fitted[38]:

$$\tau_{ave} = \frac{1}{k_r + k_{nr}}, \tag{3}$$

$$\eta_{PLQY} = \frac{k_r}{k_r + k_{nr}}. \tag{4}$$

After adding Cl-TPPO, the radiation recombination rate constant of perovskites increased from 3.29×10^7 s^{-1} to 7.32×10^7 s^{-1}, while the non-radiative recombination rate constant decreased from 1.24×10^8 s^{-1} to 5.52×10^7 s^{-1}. It was found that non-radiative recombination was strongly correlated with defects in perovskite. These results also indicated that the introduction of Cl-TPPO inhibited the formation of defects in perovskite.

To investigate the interaction between Cl-TPPO and perovskite, XPS characterization of $CsPbBr_3$ films was carried out to explore whether Cl-TPPO affected $CsPbBr_3$. The test results are shown in Fig. 3. After the addition of Cl-TPPO, the binding energies of Pb 4f orbitals and Br 3d orbitals in $CsPbBr_3$ films both shift towards lower binding energies, indicating that the addition of Cl-TPPO changed the electron cloud density around Pb^{2+} and Br^-. The decrease in binding energy corresponded to the gain of surrounding electrons. The electrons gained by Pb^{2+} came from the P═O group in Cl-TPPO, where the lone pair of electrons of the oxygen atom occupied the Pb 6p orbital[35, 39]. This interaction reduced the defect charge density of undercoordinated Pb^{2+}. The formation of the Pb—O—P bond between P═O and undercoordinated Pb^{2+} affected the binding energy of the Br 3d orbital, and the electronegativity of O is stronger than that of Br, resulting in a decrease in the binding energy of the Br 3d orbital[8].

The transient absorption (TA) spectroscopy was

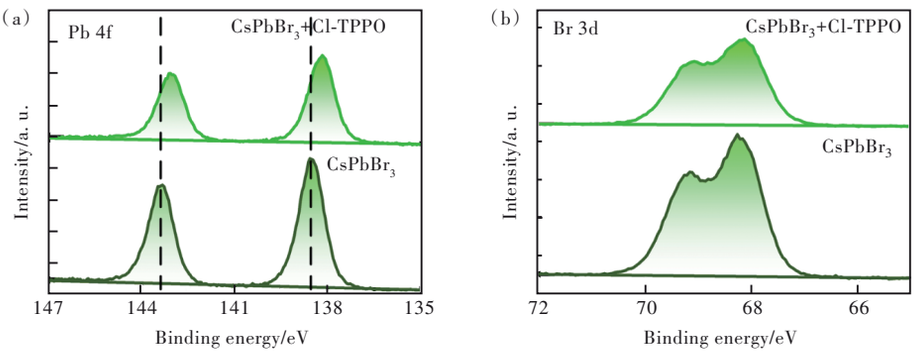

Fig.3　XPS spectroscopy of Pb 4f(a) and Br 3d(b) for different perovskite films

used to analyze the carrier dynamics in the perovskite films before and after the addition of Cl-TPPO. The test results are shown in Fig. 4. Both perovskite films, with and without Cl-TPPO, only exhibited one ground state bleaching(GSB) signal peak, consistent with the previous absorption spectroscopy results, indicating that the addition of Cl-TPPO did not change or introduce additional components. By analyzing the time evolution curve of the GSB peak in the perovskite film, it can be observed that the photogenerated carriers in the perovskite relaxed to the lowest energy state over time, resulting in a red shift of the GSB signal peak. The introduction of Cl-TPPO reduced this redshift from the initial 2.7 meV to 0.9 meV in the $CsPbBr_3$ film, indicating that the $CsPbBr_3$+Cl-TPPO film possesses a narrower energy landscape and reduced density of trap states[23,40]. This result is consistent with the previous finding that the addition of Cl-TPPO narrowed the FWHM of the perovskite film, confirming the working mechanism of Cl-TPPO in improving the performance of perovskite. The narrower energy landscape caused by the introduction of Cl-TPPO is beneficial for charge transport and radiative recombination in subsequent LED devices.

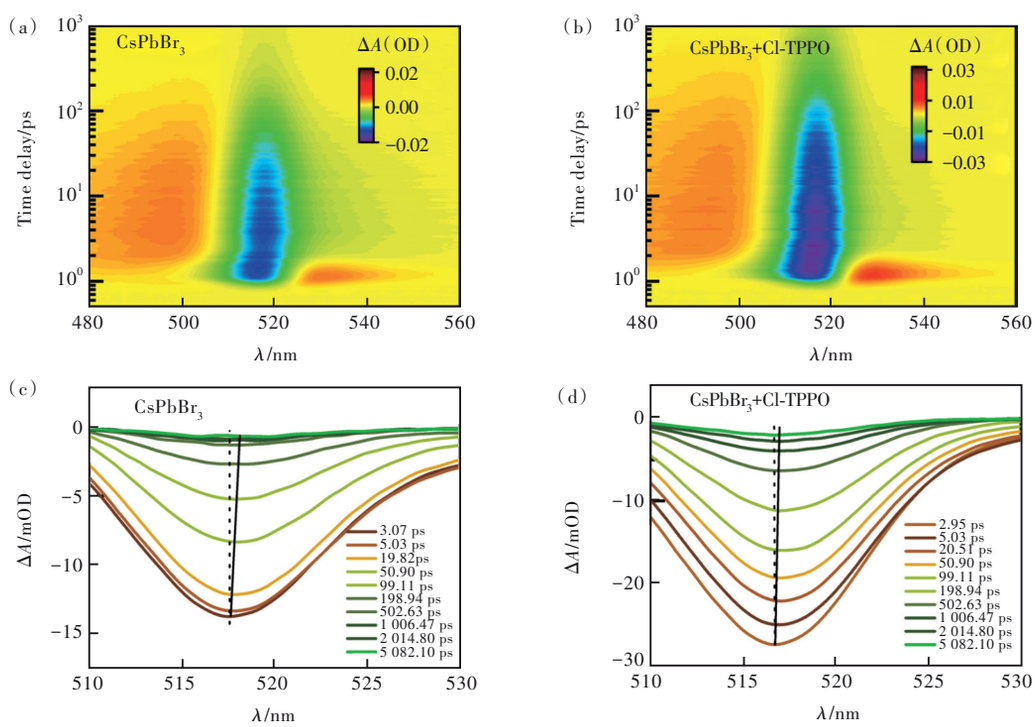

Fig.4　Pseudo color representations of TA spectra of $CsPbBr_3$(a) and $CsPbBr_3$+Cl-TPPO(b) films. TA spectra of selected pump-probe delays of $CsPbBr_3$(c) and $CsPbBr_3$+Cl-TPPO(d) films

After verifying the optimization effect of Cl-TPPO, the doping ratio of Cl-TPPO was further optimized. According to the EDS test results, we determined the doping ratio of Cl-TPPO and found that

with the increase of the Cl-TPPO doping ratio, the grain of the perovskite film gradually became smaller and the flatness of the film improved. As the Cl-TPPO doping ratio increases, the PL emission peak of the perovskite films remains relatively stable, in contrast to the peak shift observed with the mixing of Br and Cl halogens[41]. Additionally, the angle of the diffraction peaks in XRD showed minimal variation, suggesting that Cl did not significantly impact the lattice structure[42]. The main effect of Cl-TPPO is to passivate perovskite grain boundaries and serve as a ligand to decrease the defect density of the perovskites. By using Cl-TPPO passivated $CsPbBr_3$ as the light emitting layer, we constructed relevant LED devices to explore the improvement in device performance after defect passivation. As shown in Fig. 5 (a), the choice of the hole transport layer (HTL) NPB was based on the conduction band energy level of the perovskite layer, with the HOMO level of NPB positioned at 5. 5 eV. Additionally, a hole injection layer of MoO_3 was introduced to reduce the device's turn-on barrier and enhance hole injection. The structure of the LED device was ITO/MoO_3 (2 nm)/NPB (30 nm)/$CsPbBr_3$+Cl-TPPO (40 nm)/TPBi (40 nm)/LiF (1 nm)/Al (80 nm). The corresponding device performance curves are shown in Fig.5 (b) and 5 (c). Benefiting from the optimization of surface defects in the perovskite layer by Cl-TPPO, the leakage current of the device before turn-on decreased by an order of magnitude. As the current density increased after turn-on, the device brightness significantly improved, consistent with the previously verified suppression of non-radiative recombination. Ultimately, the external quantum efficiency of the device increased from an initial value of 0. 23% to 6. 3%, with a maximum brightness of 35 642 cd/m^2, making it one of the brightest devices among reported organo-inorganic hybrid perovskite LED devices prepared by thermal evaporation[24,28,30,43].

To expand the application scenarios of vacuum evaporation PeLEDs, we constructed pixelated PeLEDs based on the previously optimized 6. 3% device structure. The specific preparation process is shown in Fig. 6. First, the photoresist pixel pits were

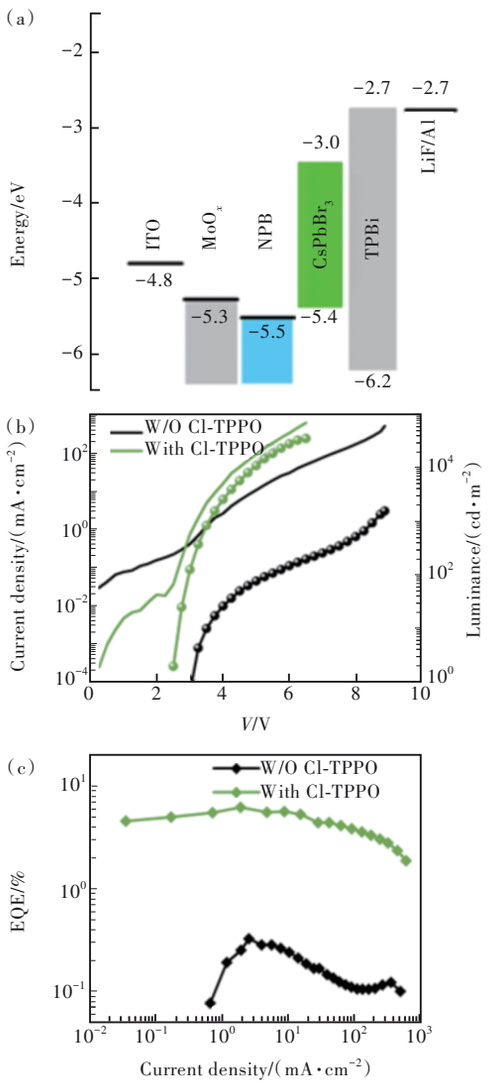

Fig.5 (a) Energy level diagram of each layer in PeLEDs. (b) Current density and luminance *versus* voltage characteristics of the PeLEDs. (c) EQE-current density curves of these two devices

prepared on the ITO substrate, and then the subsequent functional layer and perovskite layer were all deposited by vacuum evaporation. At the bottom of the pixel pit, there is ITO and the transport layer contact, and the rest of the place is blocked by the insulating photoresist, so under the voltage drive, only the perovskite layer in the pixel pit is electroluminescent (EL) to achieve pixelated PeLEDs lighting.

In the performance curve of the obtained pixelated PeLEDs shown in Fig. 7, the maximum brightness of the device is about 2 100 cd/m^2, and the maximum EQE of the device is about 5. 0%. The overall current density of the device is lower than that of the

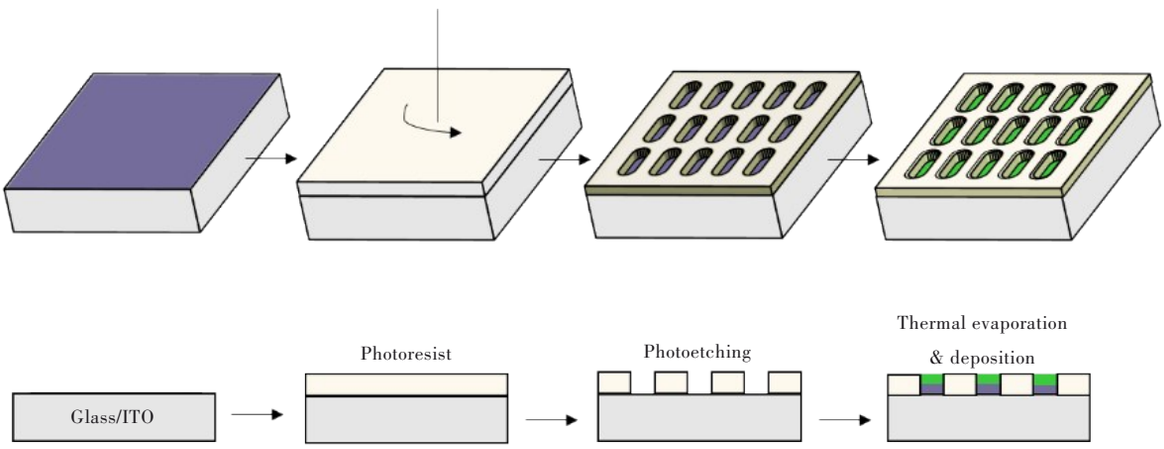

Fig.6　Flow chart of pixelated PeLEDs prepared by vacuum evaporation

PeLEDs prepared on the whole surface, which is presumably related to the possible photoresist residue at the bottom of the pixel pit, resulting in carrier injection and device brightness being affected. Fig. 7(d) shows the EL spectra of pixelated PeLEDs and a device lighting photo at 4 V, in which a single pixel pit of 60 μm × 20 μm horseshoe-shaped pixels yielded a pixelated PeLEDs resolution of 312 ppi. In addition, we collected EL intensities of 400 pixels, and their spatial uniformity is shown in Fig. S3, and the pixelated PeLED exhibits negligible intensity fluctuations, indicating the uniformity of perovskite preparation by vapor deposition of perovskites and its superiority in large-area production.

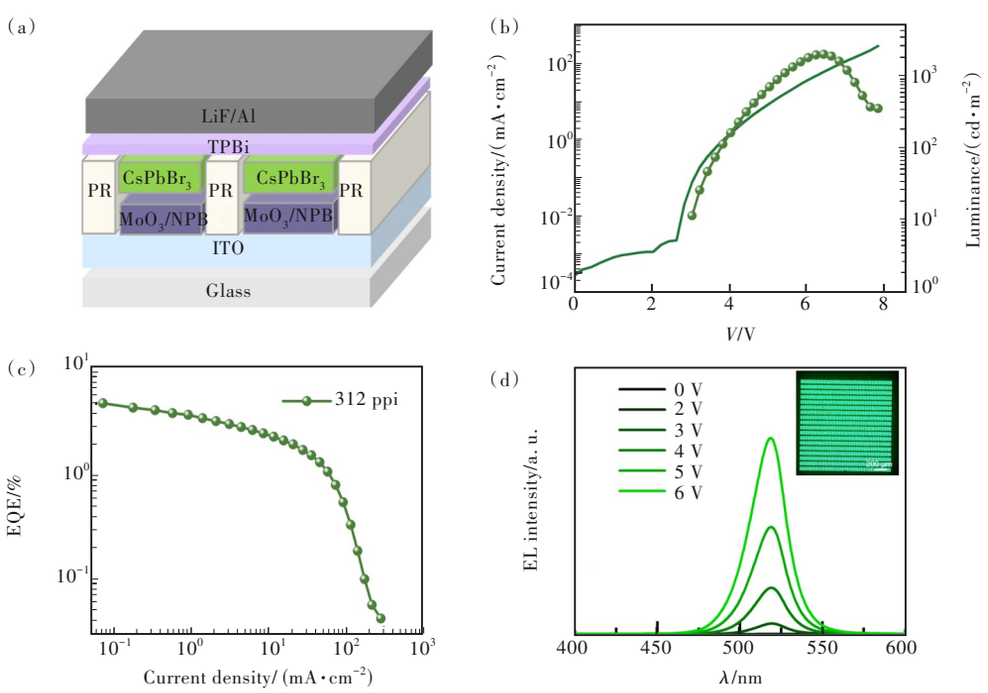

Fig.7　(a)The diagram of pixelated PeLEDs structure. (b)Current density and luminance *versus* voltage characteristics. (c)EQE-current density curves of pixelated PeLEDs. (d)EL spectra at different driving voltages of pixelated PeLEDs, the inset is the photo of pixelated PeLEDs driven at 4 V

4　Conclusion

In this work, we have reported phosphine oxide Cl-TPPO as a passivating ligand *in situ* into thermally evaporated perovskite films for efficient thermal evaporated PeLEDs. The P═O functional groups in Cl-TPPO interact with the undercoordinated Pb^{2+} ions, reducing trap density and enhancing

radiative recombination in the perovskite film, resulting in PLQY of 57%. By incorporating Cl-TPPO, the EQE of thermally evaporated PeLEDs improved from 0.23% to 6.3%, with a maximum brightness of 35 642 cd/m^2. Moreover, using the fully thermal evaporated device process, we achieved pixilated PeLEDs with an EQE of 5.0% at 312 ppi. This work explores the pixelated emission of thermally evaporated PeLEDs, highlighting the high applicability of thermal evaporation technology in the commercialization of PeLEDs for displays.

Supplementary Information and Response Letter are available for this paper at: http://cjl.lightpublishing.cn/thesisDetails#10.37188/CJL.20230231.

References:

[1] TAN Z K, MOGHADDAM R S, LAI M L, *et al*. Bright light-emitting diodes based on organometal halide perovskite [J]. *Nat. Nanotechnol.*, 2014, 9(9): 687-692.

[2] PROTESESCU L, YAKUNIN S, BODNARCHUK M I, *et al*. Nanocrystals of cesium lead halide perovskites ($CsPbX_3$, X = Cl, Br, and I): novel optoelectronic materials showing bright emission with wide color gamut [J]. *Nano Lett.*, 2015, 15(6): 3692-3696.

[3] GIL-ESCRIG L, LONGO G, PERTEGÁS A, *et al*. Efficient photovoltaic and electroluminescent perovskite devices [J]. *Chem. Commun.*, 2015, 51(3): 569-571.

[4] QUAN L N, GARCÍA DE ARQUER F P, SABATINI R P, *et al*. Perovskites for light emission [J]. *Adv. Mater.*, 2018, 30(45): 1801996.

[5] XIAO Z W, SONG Z N, YAN Y F. From lead halide perovskites to lead-free metal halide perovskites and perovskite derivatives [J]. *Adv. Mater.*, 2019, 31(47): 1803792.

[6] QUAN L N, RAND B P, FRIEND R H, *et al*. Perovskites for next-generation optical sources [J]. *Chem. Rev.*, 2019, 119(12): 7444-7477.

[7] YANG X L, ZHANG X W, DENG J X, *et al*. Efficient green light-emitting diodes based on quasi-two-dimensional composition and phase engineered perovskite with surface passivation [J]. *Nat. Commun.*, 2018, 9(1): 570.

[8] KIM J S, HEO J M, PARK G S, *et al*. Ultra-bright, efficient and stable perovskite light-emitting diodes [J]. *Nature*, 2022, 611(7937): 688-694.

[9] LIU S C, GUO Z Y, WU X X, *et al*. Zwitterions narrow distribution of perovskite quantum wells for blue light-emitting diodes with efficiency exceeding 15% [J]. *Adv. Mater.*, 2023, 35(3): 2208078.

[10] JIANG J, CHU Z M, YIN Z G, *et al*. Red perovskite light-emitting diodes with efficiency exceeding 25% realized by co-spacer cations [J]. *Adv. Mater.*, 2022, 34(36): 2204460.

[11] KIM Y H, KIM S, KAKEKHANI A, *et al*. Comprehensive defect suppression in perovskite nanocrystals for high-efficiency light-emitting diodes [J]. *Nat. Photonics*, 2021, 15(2): 148-155.

[12] MA D X, LIN K B, DONG Y T, *et al*. Distribution control enables efficient reduced-dimensional perovskite LEDs [J]. *Nature*, 2021, 599(7886): 594-598.

[13] GUO B B, LAI R C, JIANG S J, *et al*. Ultrastable near-infrared perovskite light-emitting diodes [J]. *Nat. Photonics*, 2022, 16(9): 637-643.

[14] SUN Y Q, GE L S, DAI L J, *et al*. Bright and stable perovskite light-emitting diodes in the near-infrared range [J]. *Nature*, 2023, 615(7954): 830-835.

[15] CHEN W J, HUANG Z M, YAO H T, *et al*. Highly bright and stable single-crystal perovskite light-emitting diodes [J]. *Nat. Photonics*, 2023, 17(5): 401-407.

[16] YAN F, DEMIR H V. Vacuum-evaporated lead halide perovskite LEDs [invited] [J]. *Opt. Mater. Express*, 2021, 12(1): 256-271.

[17] HAN T H, JANG K Y, DONG Y T, *et al*. A roadmap for the commercialization of perovskite light emitters [J]. *Nat.*

Rev. Mater., 2022, 7(10): 757-777.

[18] DU P P, WANG L, LI J H, *et al.* Thermal evaporation for halide perovskite optoelectronics: fundamentals, progress, and outlook [J]. *Adv. Opt. Mater.*, 2022, 10(4): 2101770.

[19] SUN C J, JIANG Y Z, CUI M H, *et al.* High-performance large-area quasi-2D perovskite light-emitting diodes [J]. *Nat. Commun.*, 2021, 12(1): 2207.

[20] YANG F, ZENG Q S, DONG W, *et al.* Rational adjustment to interfacial interaction with carbonized polymer dots enabling efficient large-area perovskite light-emitting diodes [J]. *Light Sci. Appl.*, 2023, 12(1): 119.

[21] TAN Y S, LI R Y, XU H, *et al.* Ultrastable and reversible fluorescent perovskite films used for flexible instantaneous display [J]. *Adv. Funct. Mater.*, 2019, 29(23): 1900730.

[22] ZOU Y T, CAI L, SONG T, *et al.* Recent progress on patterning strategies for perovskite light-emitting diodes toward a full-color display prototype [J]. *Small Sci.*, 2021, 1(8): 2000050.

[23] DU P P, LI J H, WANG L, *et al.* Efficient and large-area all vacuum-deposited perovskite light-emitting diodes *via* spatial confinement [J]. *Nat. Commun.*, 2021, 12(1): 4751.

[24] LI J H, DU P P, GUO Q X, *et al.* Efficient all-thermally evaporated perovskite light-emitting diodes for active-matrix displays [J]. *Nat. Photonics*, 2023, 17(5): 435-441.

[25] HU Y, WANG Q, SHI Y L, *et al.* Vacuum-evaporated all-inorganic cesium lead bromine perovskites for high-performance light-emitting diodes [J]. *J. Mater. Chem.* C, 2017, 5(32): 8144-8149.

[26] GENCO A, MARIANO F, CARALLO S, *et al.* Fully vapor-deposited heterostructured light-emitting diode based on organo-metal halide perovskite [J]. *Adv. Electron. Mater.*, 2016, 2(3): 1500325.

[27] DÄNEKAMP B, DROSEROS N, PALAZON F, *et al.* Efficient photo- and electroluminescence by trap states passivation in vacuum-deposited hybrid perovskite thin films [J]. *ACS Appl. Mater. Interfaces*, 2018, 10(42): 36187-36193.

[28] SONG L, HUANG L X, LIU Y, *et al.* Efficient thermally evaporated perovskite light-emitting devices *via* a bilateral interface engineering strategy [J]. *J. Phys. Chem. Lett.*, 2021, 12(26): 6165-6173.

[29] DU P P, LI J H, WANG L, *et al.* Vacuum-deposited blue inorganic perovskite light-emitting diodes [J]. *ACS Appl. Mater. Interfaces*, 2019, 11(50): 47083-47090.

[30] HSIEH C A, TAN G H, CHUANG Y T, *et al.* Vacuum-deposited inorganic perovskite light-emitting diodes with external quantum efficiency exceeding 10% *via* composition and crystallinity manipulation of emission layer under high vacuum [J]. *Adv. Sci.*, 2023, 10(10): 2206076.

[31] KIM Y H, PARK J, KIM S, *et al.* Exploiting the full advantages of colloidal perovskite nanocrystals for large-area efficient light-emitting diodes [J]. *Nat. Nanotechnol.*, 2022, 17(6): 590-597.

[32] CHEN Z M, LI Z C, ZHANG C Y, *et al.* Recombination dynamics study on nanostructured perovskite light-emitting devices [J]. *Adv. Mater.*, 2018, 30(38).

[33] AKKERMAN Q A, RAINÒ G, KOVALENKO M V, *et al.* Genesis, challenges and opportunities for colloidal lead halide perovskite nanocrystals [J]. *Nat. Mater.*, 2018, 17(5): 394-405.

[34] ZHAO B D, LIAN Y X, CUI L S, *et al.* Efficient light-emitting diodes from mixed-dimensional perovskites on a fluoride interface [J]. *Nat. Electron.*, 2020, 3(11): 704-710.

[35] LI M L, ZHAO Y P, QIN X Q, *et al.* Conductive phosphine oxide passivator enables efficient perovskite light-emitting diodes [J]. *Nano Lett.*, 2022, 22(6): 2490-2496.

[36] CHU Z M, YE Q F, ZHAO Y, *et al.* Perovskite light-emitting diodes with external quantum efficiency exceeding 22% *via* small-molecule passivation [J]. *Adv. Mater.*, 2021, 33(18): 2007169.

[37] BAN M Y, ZOU Y T, RIVETT J P H, *et al.* Solution-processed perovskite light emitting diodes with efficiency exceeding 15% through additive-controlled nanostructure tailoring [J]. *Nat. Commun.*, 2018, 9(1): 3892.

[38] ZHAO C Y, WU W P, ZHAN H M, *et al.* Phosphonate/phosphine oxide dyad additive for efficient perovskite light-emitting diodes [J]. *Angew. Chem. Int. Ed.*, 2022, 61(13): e202117374.

[39] LI M L, ZHAO Y P, GUO J, *et al.* Phase regulation and defect passivation enabled by phosphoryl chloride molecules for

efficient quasi-2D perovskite light-emitting diodes [J]. *Nanomicro Lett.*, 2023, 15(1): 119.

[40] WANG H R, ZHANG X Y, WU Q Q, *et al*. Trifluoroacetate induced small-grained $CsPbBr_3$ perovskite films result in efficient and stable light-emitting devices [J]. *Nat. Commun.*, 2019, 10(1): 665.

[41] WANG X C, BAI T X, MENG X, *et al*. Filling chlorine vacancy with bromine: a two-step hot-injection approach achieving defect-free hybrid halogen perovskite nanocrystals [J]. *ACS Appl. Mater. Interfaces*, 2022, 14(41): 46857-46865.

[42] MCGRATH F, GHORPADE U V, RYAN K M. Synthesis and dimensional control of $CsPbBr_3$ perovskite nanocrystals using phosphorous based ligands [J]. *J. Chem. Phys.*, 2020, 152(17): 174702.

[43] WANG L, LI J H, DU P P, *et al*. Effect of post-annealing on thermally evaporated reduced-dimensional perovskite LEDs [J]. *Appl. Phys. Lett.*, 2022, 120(8): 081107.

刘念(1997-),女,湖北天门人,博士研究生,2018年于华中科技大学获得学士学位,主要从事热蒸发技术制备钙钛矿发光二极管的研究。
E-mail: nianl_hust@hust.edu.cn

唐江(1981-),男,湖南浏阳人,博士,教授,2010年于多伦多大学获得博士学位,主要从事量子点红外探测芯片、卤素钙钛矿X射线探测器和卤素钙钛矿发光材料与器件的研究。
E-mail: jtang@mail.hust.edu.cn

罗家俊(1993-),男,湖北武汉人,博士,副研究员,2020年于华中科技大学获得博士学位,主要从事新型发光材料与显示技术的研究。
E-mail: luojiajun@hust.edu.cn